ACM Symposium on Solid Modeling and Applications (2004)
G. Elber, N. Patrikalakis, P. Brunet (Editors)

B-rep SE: Simplicially Enhanced Boundary Representation

Michael Freytag and Vadim Shapiro†

Spatial Automation Laboratory
University of Wisconsin-Madison

Abstract

Boundary representation (B-rep) is a popular representation scheme for mechanical objects due to its ability to accurately represent piecewise smooth surfaces bounding solids. However, non-trivial topology and geometry of the surface patches hinder point generation, classification, searching, and other algorithms. We propose a new hybrid representation that addresses these shortcomings by imposing on the boundary representation an additional simplicial structure. The simplicial structure applies a triangle-mesh metaphor to the usual boundary representation, allowing access to points on the exact solid boundary or its many approximations. The resulting simplicially enhanced boundary representation (B-rep SE) simplifies and accelerates the usual boundary representation queries. We discuss full implementation of B-rep SE with the Parasolid kernel and demonstrate the advantages of B-rep SE in applications that integrate and visualize arbitrary fields on a solid's boundary.

1. Introduction

Classical, non-tessellated, boundary representations (B-reps) and triangular meshes have complementary properties. The boundary representation for artifacts in engineering applications is usually conceptualized as a cell complex in $\mathbb{E}^3$ with faces represented by trimmed parametric surfaces, edges by parametric curve segments, and vertices by points. B-reps, see Figure 1 (a), thus have arbitrary accuracy and smoothness that lead to slow queries implemented in proprietary, high resolution geometric engines. In contrast, a triangular mesh is a particular type of B-rep that uses triangles, line segments, and points to represent faces, edges, and vertices respectively. Mesh approximations of exact B-reps, see Figure 1 (b), are typically constructed to support rapid query computation through widely available tools in a multi-resolution framework. Unfortunately, triangular meshes have finite, fixed accuracy and lack the smoothness of non-tessellated B-reps.

1.1. Queries with B-reps and Meshes

Engineering applications that compute with solids frequently require *point generation*. Point generation involves the distribution of points on the geometric boundary in a controlled fashion for tasks such as rendering, numerical integration[MM97], or meshing. Most of the work in this area has been in the generation of points on exact B-reps for meshing, including techniques for decomposition of a solid's faces into manageable pieces[KSSP01], distribution of points based on surface differential properties[CB97, KS95, SYI97, Pet94], or vertex insertion based on geometric measures of mesh angles and edge lengths[VB93, SH93]. Other algorithms recursively subdivide the parametric domains of the faces with a quadtree[Sam84] until the segment of the face within each cell is unambiguous, or meets flatness criteria[FK90]. Typically, once the parametric domains for the faces have been suitably decomposed, they are triangulated, the triangles are mapped to $\mathbb{E}^3$, and the parametric decompositions are discarded. Generation algorithms are frequently slowed when faces with non-trivial topology and non-planar geometry are encountered. As demonstrated in [KSSP01, RHD89], significant computational overhead is required to decompose faces possessing non-trivial topology and geometry into regions that lend themselves to treatment by some standardized algorithm. With triangular meshes, however, all cells of a given dimension possess the same topology and similar geometry so their interiors are easily parameterized using barycentric coordinates and generated points are simply convex combinations of appropriate vertices.

Classification is the answering of queries involving a point and geometric boundaries. Examples include membership (in/out/on) and distance (to nearest boundary point). For B-reps, the popular algorithms for classification queries involve iterative Newton-type methods that operate on the the parametric geometry describing a solid's boundary[Mor97]. With

† Complete address: 1513 University Avenue, Madison, WI 53706, USA. E-mails: vshapiro@engr.wisc.edu, mkfreytag@wisc.edu

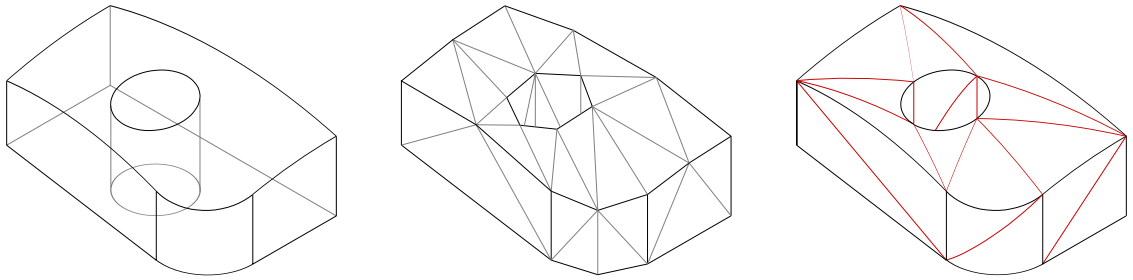

(a) (b) (c)

Figure 1: ***Three representations.*** *(a) Shows a B-rep solid with curved faces; the top face containing a hole and curved edges. (b) Shows a mesh approximation of the same solid as in (a). (c) Depicts simplicial enhancement of the B-rep from (a). The additional curved edges are logical incidence links between points on the boundary.*

triangular meshes, point membership classification by ray-boundary intersection is rapid since ray-cell intersections have closed form solutions. Even faster techniques take advantage of signed triangles or enclosing tetrahedra sharing a common vertex whose membership is known [FTU95]. Distance computations against meshes are further accelerated through pre-processing with 3D bucket sorting techniques [CLR90]. Of course classification algorithms against meshes still produce results that are only as accurate as the resolution of the mesh approximation. As Figure 2 shows, attempts to refine mesh approximations to curved surfaces will generate new vertices that lie, not on the exact surface where we would like, but on the original polyhedral approximation to the surface.

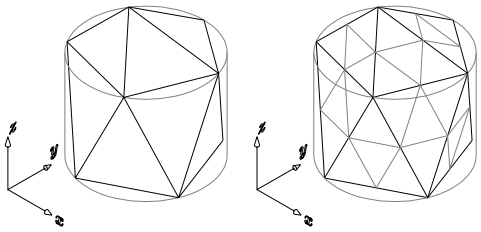

Figure 2: ***Nonconforming mesh subdivision.*** *This figure shows how refinement of a triangular mesh by subdivision will not conform to exact geometry that is curved.*

B-reps constructed from exact parametric geometry do not lend themselves to direct treatment in a multi-resolution framework possessing varying levels of geometric detail. The complex adjacency relationships among the intersecting faces are not easily maintained when faces are approximated by simpler geometry. To enable multi-resolution treatment, mesh approximations of B-reps are created. Meshes support the creation of multi-resolution representations including ones with levels of detail defined relative to one another in a hierarchical structure[FP95, Hop96, GH98a]. Most of these multi-resolution approximations are constructed by a sequence of decimation steps that generate models at different levels of accuracy. Association of cells among levels produces the hierarchy of meshes, each with increasing levels of accuracy. Such structures speed up classification algorithms by providing good starting points after fast localizing computations that cull non-candidate elements in the mesh. The remaining candidate elements map to a set of more accurate candidates where the culling operation is repeated[Sab01, O'R98]. Subdivision surfaces[SZD*98, Sab02], in a sense, invert the multi-resolution paradigm by starting with coarse meshes. Through the generation of progressively finer resolutions, subdivision surfaces build up arbitrary levels of accuracy and smoothness, defined by application of specific subdivision rules. Subdivision surfaces are thus easily stored and exchanged, with arbitrary precision and smoothness available by application of the subdivision rules.

1.2. B-rep SE

We propose that the traditional boundary representation be enhanced by combining the attractive properties of both exact B-reps and triangular meshes. The resulting hybrid representation, called B-rep SE, possesses many of the computational advantages of subdivision surfaces. By inducing on the exact B-rep, a simplicial structure that contains the same geometric information as the B-rep, the B-rep's accuracy and smoothness is retained while providing the speed (through approximation and multi-resolution) and simplicity (identical cell topology, similar geometry) of triangular meshes. Figure 1(c) shows simplicial enhancement of the B-rep from Figure 1(a). The simplicial structure provides spatial addressing, with exact and approximate representations of the solid arising as particular geometric realizations of the simplicial structure. By defining a correspondence between points in the exact and approximate realizations, approximation error can be quantified and subdivision carried out to generate adaptive approximations that converge to the exact B-rep in the limit.

The remainder of this paper is organized as follows. In Section 2 we discuss the conceptual structure of the B-rep SE as well as some of the issues in its implementation in a computer data structure. In Section 3, we discuss application of the B-

rep SE to geometry visualization as well as visualization and integration of *externally defined* scalar fields on the boundary of solids. We finish with some concluding remarks and suggestions for future work.

2. B-rep SE Concepts

To combine the attractive properties of both the B-rep and the triangular mesh, we need a common formal framework that applies to both structures. Since B-reps and meshes are both cell complexes, they share a common foundation in the realm of abstract complexes. The simplest of these abstract complexes are the abstract *simplicial* complexes which conveniently represent the topology of meshes. We induce such a simplicial structure on the B-rep to create the B-rep SE. We discuss the B-rep SE in detail, following an introduction to some supporting terminology and definitions.

2.1. Definitions and Components

We consider a boundary representation S as a complex of closed cells in $\mathbb{E}^3$. 2-cells in this complex are faces, 1-cells are edges, 0-cells are vertices. To represent S we use Parasolid[UGS]; however, any appropriate data structure can be used. The cells of S are not necessarily homeomorphic to a ball, but are smooth manifolds of appropriate dimension. Because the cells of S form a complex, any two cells either intersect on another cell in the complex or are disjoint. We choose to define our B-rep as a complex of closed cells as this simplifies our ensuing definitions.

In order to combine meshes and B-reps, they need to be defined in the same space. However, linear meshes are defined in $\mathbb{E}^3$ whereas B-reps are defined as mappings from parametric space to $\mathbb{E}^3$. Further, meshes do not generally define the same pointset as the B-rep. Fortunately, both B-reps and meshes have a common denominator in an *abstract cell complex*. An abstract complex, A, is a finite set of elements $a^0, a^1, \ldots$, called (*abstract*) *vertices*, together with a collection of subsets $(a^{i_0}, a^{i_1}, \ldots, a^{i_n}), \ldots$, called (*abstract*) *faces*, with the property that any subset of a face is itself a face. When every face is a simplex, a simplicial complex results. The dimension of an abstract simplex is one less than the number of vertices in it, and the dimension of A is the maximum of the dimensions of its simplexes[HY88, Mau80]. Figure 3 illustrates the idea behind an abstract simplicial cell complex. Essentially, an abstract complex takes a collection of abstract vertices and assigns logical incidence among them. We use simplicial complexes because they embed naturally as triangular meshes.

The cells of S can have arbitrary topology and geometry; however, because they are smooth manifolds, they are triangulable[Lee00, Cai68, Req77]. The connectivity of such a triangulation is key to the simplicial enhancement of S:

Definition 1 A *simplicial enhancement* $E = (A, g)$ of a B-rep solid S is an abstract simplicial cell complex A, and a *vertex map* $g : A \to S$ with the following properties:

1. For every 0-simplex a in A, $g(a)$ is a unique point on the boundary of S.
2. g can be extended (non-uniquely) to an embedding g^* such that every cell in S is the union of some simplexes in $g^*(A)$.

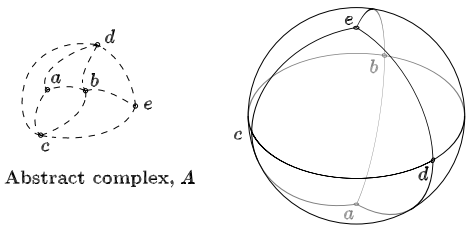

Figure 3: ***Abstract complex and embedding.*** *This figure shows a simplicial complex A consisting of 0-simplexes $\{a, b, c, d, e\}$ along with their logical incidence edges. 1-simplexes in this complex are: $\{ad, ab, ac, bd, bc, be, cd, ce, de\}$ and 2-simplexes are: $\{abd, adc, acb, bce, bed, dce\}$. On the right is shown a simplicial enhancement of a sphere (A, g) using a particular embedding g^*.*

Figure 3 shows a simplicial enhancement of a sphere (A, g) for a particular embedding g^*.

2.2. B-rep SE

Definition 2 A *B-rep SE* is a pair: (S, E), where S is a B-rep representation of a solid and E is an associated simplicial enhancement of S.

From Definition 2 we have a finite set of points on S with the abstract simplicial complex, A, assigning incidence among them. The arbitrarily shaped cells of S are now the union of cells in a triangulation of S, so navigation over S is by traversal of the simplexes as a graph. The idea of having a set of vertices with explicit connectivity is similar to subdivision surfaces [Sab02] except in our case the exact surface is defined not as the limit of a subdivision process; rather it is the underlying geometry of the boundary representation. We are thus able to construct application-specific subdivision rules that depend not on the geometry of the mesh, but on a variety of controls such as globally defined fields, local measures of mesh accuracy, or surface curvature, among others. Further, vertices inserted during subdivision will lie precisely on S. In Section 3, we discuss subdivision based on both field interpolation error and deviation of mesh geometry from corresponding exact surfaces.

Just like with subdivision surfaces, the simplicial structure of the B-rep SE may be used to induce an approximation of the exact embedding. The most popular and important approximation is a piecewise linear approximation constructed by taking convex combinations of the vertices of each embedded 2-cell from A. The result is a triangular mesh approximation of S. The vertices of this approximation will lie on S and have edges corresponding to the connectivity of A. This mesh can be used in place of the exact boundary representation, assuming a close correspondence exists between the two representations.

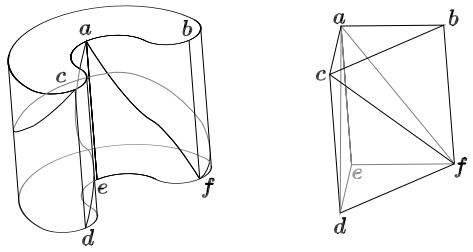

Figure 4: ***Invalid approximation of an embedding.*** *On the right is an example of an invalid mesh (improper orientation) produced by an approximation of the embedding g^* shown on the left.*

Note that a triangular mesh constructed in the above manner may not have the same topology as S unless the embedded 0-simplexes are sufficiently close to one another. For example, the mapping from the exact surface to the approximation may not be an embedding because the mapping is not *1-to-1*. Even if the mapping is an embedding the resulting approximation may not have the same orientation as the exact boundary representation (see Figure 4 for an example). For many (but not all) engineering purposes, such approximations are not valid; however even invalid approximations may be refined by subdivision into a valid approximation of the boundary representation.

From the conceptual structure presented here, some useful consequences arise. The B-rep SE has the usual smoothness and completeness properties of a B-rep plus some additional capabilities. The addition of the simplicial structure improves spatial addressibility of the boundary of S since the interiors of the cells of S are now simplicially decomposed and could be parameterized for point generation. The usual advantages of meshes (multi-resolution and rapid classification) also apply with the full accuracy of the B-rep available for refinement operations. Below, we discuss how these operations may be implemented with a typical B-rep SE.

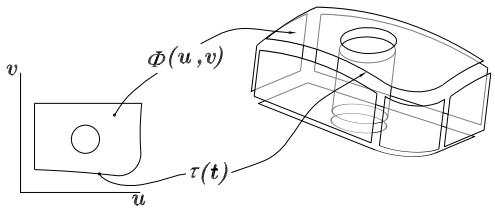

Figure 5: ***B-rep data structure.*** *This figure illustrates the conventional B-rep data structure. Faces are represented by trimmed parametric surfaces, $\Phi_i(u,v)$. Each edge, the intersection of adjacent faces, is represented by the trim curves, $\tau_{j,i}(t)$, in the parametric space of the adjacent faces as well as by a parametric curve in $\mathbb{E}^3$.*

2.3. B-rep SE Implementation

The conventional data structure for representing our B-rep solid S is depicted in Figure 5. The faces of S are represented by parametric surfaces whose parameter domain is bounded by trim curves. Points within the domain evaluate to points on S. In practice, trim curves are usually approximated within some tolerance. Our work does not address these tolerance issues; we allow the modeling engine to deal with the representation of geometry at its own level of accuracy.

To represent A, we need a data structure that captures the incidences among the vertices of A and enables efficient computation of the vertex map $g(A)$ as well as its extension, $g^*(A)$. As depicted in Figure 6, the vertex incidences of A may be represented by edges in triangulations of the parametric domains of the solid's surfaces. $g(A)$ can be computed through the evaluation of the parametric surface function at the vertices of these triangulations. Points in the extension, $g^*(A)$, can be similarly computed by evaluating points within the edges and faces of these triangulations. In our implementation A is received from the modeling kernel as triangulations of the parametric domains, constructed using the kernel's built-in tessellation routines. The trim curves are represented in piecewise linear fashion by edges in the data structure. When requesting the triangulations from the kernel, we specify that valid connectivity of the triangulations across the solid's edges be enforced. Because we approximate the trim curves by linear segments, there will be some error when computing $g^*(A)$ in the vicinity of parametric boundaries. The error introduced by this approximation is controlled by specifying an error tolerance when calling the kernel's tessellation subroutine. This tolerance can be adjusted based on application-specific accuracy requirements.

2.3.1. Approximations and Correspondence

Approximations of $g^*(A)$ are useful for a variety of tasks like visualization, classification, and rendering. The most familiar approximation is the triangular mesh, constructed from the vertices of $g(A)$, connected using line segments and planar triangles in $\mathbb{E}^3$ according to the incidence in A. As Figure 6 suggests, higher resolution mesh approximations are constructed by evaluating and connecting more points from the interior of cells of $g^*(A)$.

Correspondence mappings can be defined and constructed between points in $g^*(A)$ and its approximations. A straightforward means of accomplishing this is to take advantage of the representation of A in the parametric domain of the faces of S. When A is represented using a linear triangulation in the parametric domain, barycentric coordinates can be used to identify corresponding points in both $g^*(A)$ and its approximation on a per-cell basis. Thus, we define points in the approximation and points in $g^*(A)$ to correspond if they possess the same barycentric coordinates. Obviously, other methods of correspondence computation can be used depending on application. We choose the barycentric basis because it is efficient and is a natural extension of our representation of A. In the conclusion, we briefly discuss higher order approximations of $g^*(A)$ as well as other types of correspondences.

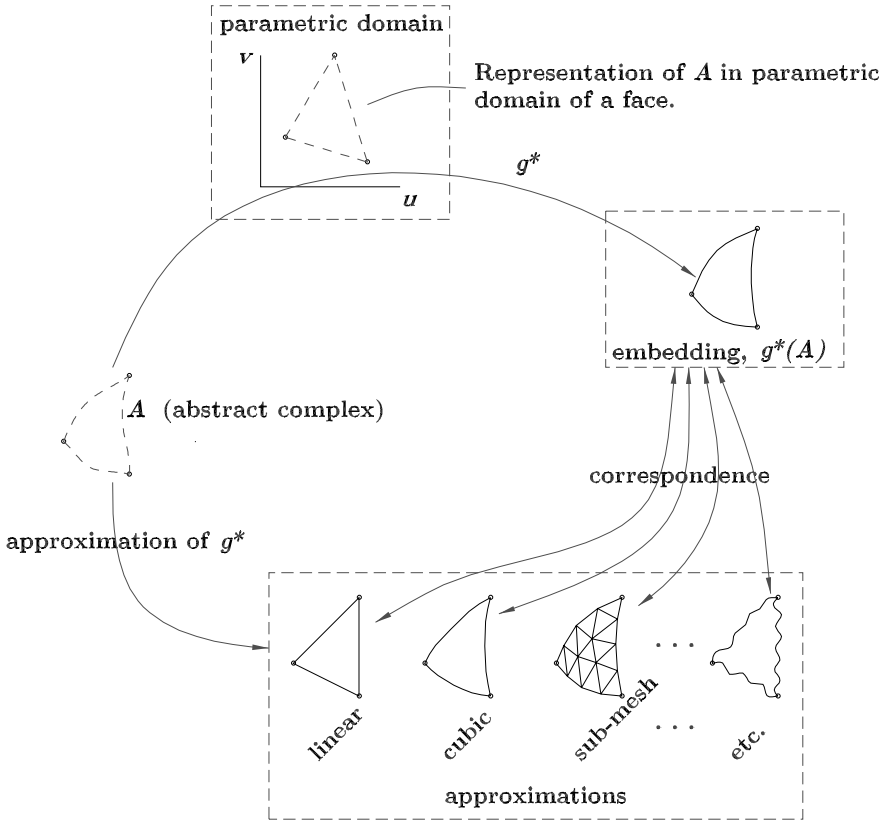

Figure 6: ***A representation of B-rep SE.*** *The abstract complex, A, can be represented using triangulations of the parametric domains of a solid's faces (a single 2-simplex is shown for clarity). To the right is the extension of the vertex map to an embedding, $g^*(A)$, computed through the parametric surface equation. At the bottom are approximations of the embedding. Correspondence functions map points between the embedding and its approximations.*

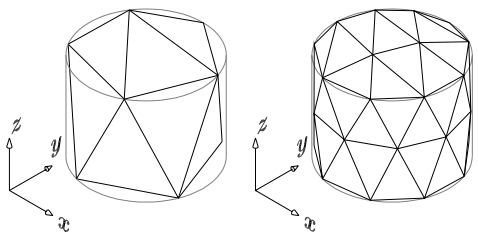

Figure 7: ***Refinement by subdivision.*** *This figure shows how subdivision of the abstract complex A refines the mesh approximation of S with new vertices that lie on S.*

2.3.2. Refinement

Approximations of $g^*(A)$ may be invalid or have insufficient accuracy as measured by some defined correspondence. Refined approximations can be constructed by increasing the density of the embedded vertices, thereby increasing the resolution of the approximation. A natural way to refine the B-rep SE is through subdivision as shown in Figure 7. Subdivision of A produces a new complex A' with more vertices and abstract simplices, resulting in smaller edges and triangles in the approximation. The embedding of this new complex will still have vertices that lie on S but they will be closer together. If the correspondence mapping is bijective and meets the Lipschitz condition (i.e., $|h(x_1) - h(x_0)| \leq K|x_1 - x_0|$ for some constant K, where $h(\cdot)$ is the correspondence map), we can expect approximations to converge to the embedding $g^*(A)$ in the limit. The Lipschitz condition places a bound on the distance that the embedding will deviate from its approximation. Since the vertices of $g(A)$ are in the approximation of $g^*(A)$, as the distance between vertices shrinks, so does the maximum deviation of the embedding from it's approximation. The ability to make the error arbitrarily small is a capability that is useful in sampling and approximation applications.

Through subdivision, mesh approximations are thus arbitrarily refineable. In other words, points on the boundary can be generated with arbitrarily small separation, and their interpolation can be made arbitrarily close to the exact boundary. In

contrast, (apart from subdivision surfaces) subdivision of traditional triangular meshes introduces vertices that only lie on the geometry of the original mesh approximation (see Figure 2). However, unlike subdivision surfaces, subdivision of B-rep SE can adapt locally or globally in a manner that is best suited to a particular task or application, always leaving the original surface itself unchanged.

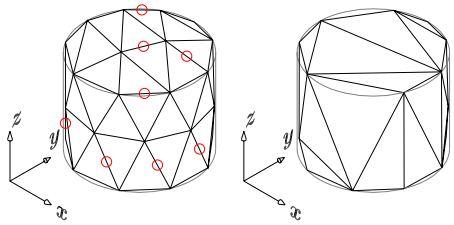

Figure 8: ***Coarsening.*** *This figure shows how the density of the vertices in the piecewise linear approximation of S can be reduced through the collapse of 1-simplexes of A. The edges marked with the circles have been collapsed to produce the complex on the right.*

2.3.3. Coarsening

Coarsening is the removal of simplexes from A to reduce the number of vertices in its embedding. As shown in Figure 8, the collapse of a 1-simplex removes one 0-simplex (vertex), three 1-simplexes (edges), and two 2-simplexes (faces) from A. However, unlike edge collapses as applied to triangular meshes[GH97], coarsening of A through collapses of 1-simplexes involves no loss of information since new vertices can always be inserted by subdivision. Any 1-simplex can be collapsed so long as the conditions on simplicial enhancement (Def. 1) are not violated. The conditions of Def. 1 ensure that $g^*(A)$ will always cover the solid boundary and enable subsequent recovery of the full B-rep accuracy.

Additional restrictions on the collapse of 1-simplexes are imposed by the data structure we choose to represent A. For example when A is represented by planar triangulations in the parametric space of the solid's faces, any collapses must maintain validity of this triangulation. The triangulations must continue to cover the parametric domain with properly oriented, non-overlapping triangles. Representation of the trim curves by linear segments may also prevent collapse of these edges depending on the accuracy required by an application. Restrictions may be imposed by the parametric surface itself if it is periodic or contains degeneracies that govern the orientation and connectivity of edges in its parametric triangulation.

Repeated coarsening steps up to the limits imposed by Def. 1 and representation of A suggests the notion of *minimal* simplicial enhancements that retain the full accuracy of the B-rep while possessing a minimum number of simplexes. Obviously, such minimal structures are not unique since there are many ways to triangulate a manifold. However, all such structures contain the same information: they introduce minimal overhead to the original B-rep while enhancing it with subdivision capabilities.

3. Application of B-rep SE

In this section we discuss application of the B-rep SE to adaptive geometry visualization, adaptive field visualization, and surface integral computation. In the conclusion we propose other applications for the B-rep SE. We discuss how its capability for arbitrary refinement and coarsening can be applied in any environment where multi-resolution representations have application.

3.1. Geometry Visualization

Geometry visualization is important in the design process to get visual feedback of part shape as changes are made. Since graphics engines typically accept geometry data in the form of triangular meshes, we need a way to generate triangular mesh approximations of our solids. Many algorithms exist for generating triangular meshes of solids, and it is a standard operation in solid modeling engines. With the B-rep SE, we can generate meshes for display and locally adapt them to more accurately represent the exact geometry they depict. Using the notion of correspondence, we can also quantify the error in the mesh approximation of the exact solid. Further, through refinement and coarsening steps, the accuracy can be locally adapted based on the measured error.

For example, our implementation of geometric visualization follows a system inspired by Velho et al in [VdFG99]. In their work the coherency of hierarchical mesh approximations to parametric surfaces is maintained by subdivision of triangles according to templates that are chosen after finding those edge points having maximum deviation from the surface. Occasionally triangle interiors are randomly sampled and subdivided as well. As in Velho's work, we carry out adaptation of 1-simplexes first since the error maximization process takes the form of a simple 1-D search problem. Error at points in the mesh approximation is measured by the Euclidean distance, $\delta = ||x^* - h(x^*)||$, where x^* is a point on the linear approximation of the embedding and $h(x^*)$ is the corresponding point on the embedding. Where δ is a maximum and greater than a user-specified threshold, the 1-simplex is subdivided. By processing all existing 1-simplexes in a single step, better aspect ratios for the approximating triangles result and geometric accuracy generally improves more rapidly with fewer subdivisions. 1-simplex subdivision is complete when all errors are below the user-specified geometric error threshold. After 1-simplex subdivision has finished, adaptation can be performed within 2-simplexes to ensure geometric detail is fully captured. The cycle is repeated until no more subdivisions are required. The results of several cycles of this process are shown in Figure 9.

With the B-rep SE, geometry visualization can be viewed as "triangulation on demand" in the sense that triangular meshes are not used as archival representations. They are generated only when required by a particular application and with accuracy that is needed to answer particular queries. Just like with B-rep, arbitrary resolution is available at any time, but simplicial enhancement allows rapid generation of triangular mesh approximations with local control of accuracy.

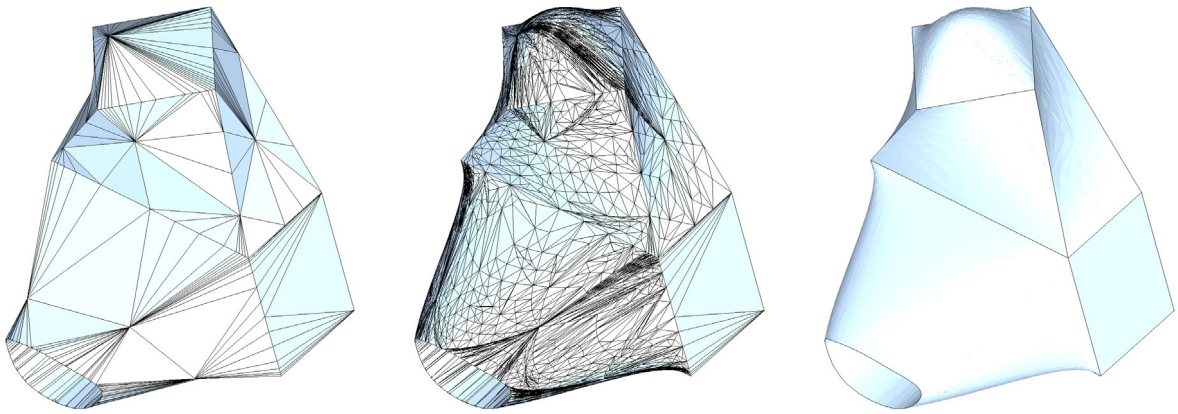

(a) (b) (c)

Figure 9: ***Adaptation to geometry.*** *On the left is a flat-shaded coarse mesh approximation of a solid boundary constructed using B-rep SE. On the right is another flat-shaded mesh of the same geometry adaptively subdivided based on geometric error. The algorithm subdivides mesh edges where their deviation from the embedding is a maximum and greater than a user-specified tolerance. Notice in the center figure the resulting concentration of triangles in regions of high curvature, and relative sparseness in planar regions.*

3.2. Field Visualization

Fields are spatially distributed quantities that usually have some physical interpretation such as temperature, pressure, fluid flow, stress, or strain. In engineering, these fields may be either measured physically through testing or computed through analysis. Using visualization tools, engineers interpret the interaction of these fields with geometry. We are especially interested in *externally defined* fields– fields whose values do not depend on a particular decomposition of the solid boundary. Such fields arise, for example, in meshless analysis[TS02], material modeling[BST03], and in computations involving fields with differing underlying representations. In other applications, the solid may be simply used as a "probe" into the field. The boundary of the solid then provides a surface onto which field values are mapped for display.

Field visualization generates human-readable images allowing interpretation of field values on the boundary of the solid. The approach requires that points be generated on the solid where the field can be sampled. The samples are then mapped to hues, and their positions projected for display. The projection of all visible sample points by ray-casting is too computationally intensive to allow interaction with the model. Instead, hardware acceleration is used to display a mesh approximation of the solid. The field is sampled at the vertices of the mesh, and the hardware linearly interpolates the corresponding hues over the triangle interiors.

In traditional general-purpose visualization applications a triangular mesh is used exclusively. To ensure details in the field and the geometry are adequately captured, high resolution meshes must be employed. However, such high-resolution meshes hinder interaction by slowing the rendering process. Furthermore, as Figures 10 (a) and (b) illustrate, much of the mesh density can be wasted in regions where the field is relatively uniform. To reduce overhead, the meshes can be decimated, reducing triangle count where geometric and field accuracy is not affected significantly by removal of triangles. Techniques like those of Hoppe [Hop99] and Garland [GH98b] can take into account appearance attributes, but to use these techniques successfully we still must start with a high-resolution mesh. Adaptation to new field details after decimation is not a trivial process, nor is it possible to quantify the error introduced by linear interpolation of either the field or the geometry.

Visualization with the B-rep SE uses a mesh constructed directly from an approximation of the embedding of A. To extend the idea of adaptation to geometry to include adaptation to fields, we measure interpolation error as the difference between the linearly interpolated field values at points on the linear mesh and the actual field values sampled at corresponding points on the exact geometry. The accuracy can be locally adapted based on these errors. Thus, without preprocessing, we can zoom in to arbitrary levels of detail, increasing vertex density only where required. As with adaptation to geometry, all necessary 1-simplex subdivisions are carried out simultaneously. Figure 10 (c) shows a mesh adaptively refined to display the same field as in Figure 10 (b). The difference in display quality between the two techniques is negligible, but there are 98K triangles in (b) while there are only 6K triangles in (d). Further, the sample spacing used during the adaptation of the B-rep SE is more than ten times finer than the resolution available by using the fine mesh in (a).

Adaptation of the B-rep SE for visualization involves the refinement of the simplicial complex to capture the curvature in the field and in the geometry. Because the spatial variations of the field and the curvature of the geometry do not necessarily correspond, we must adapt to both. For example, as Fig-

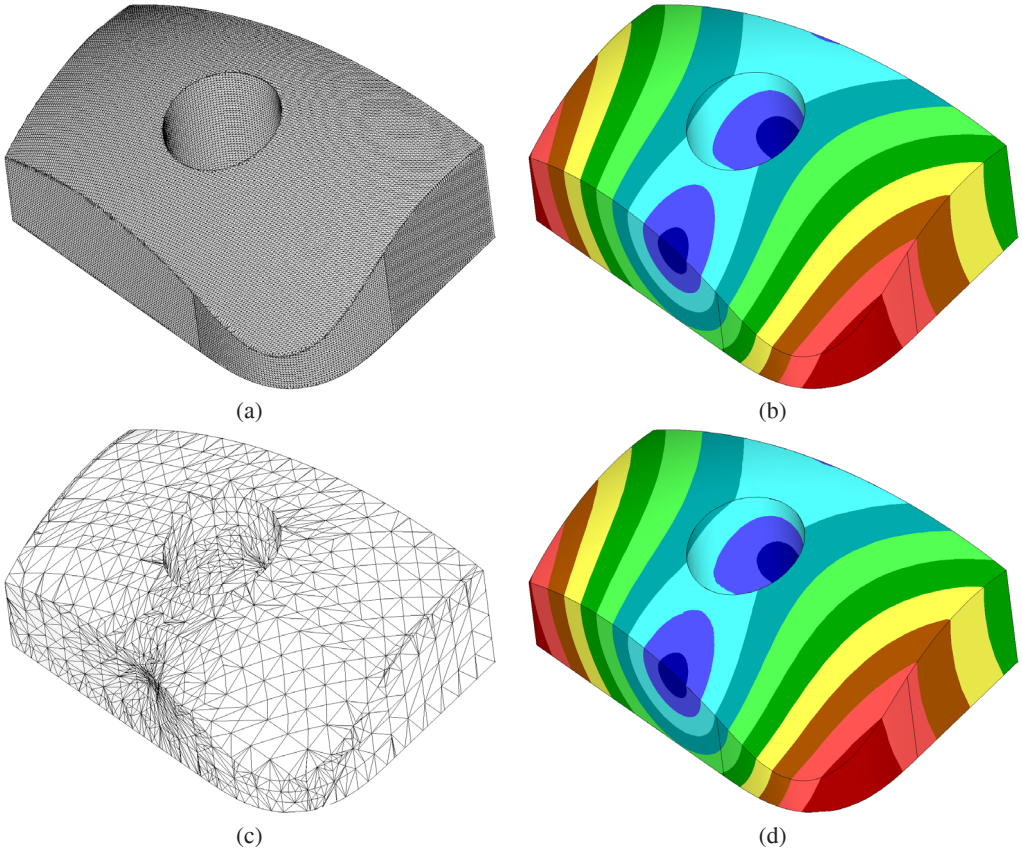

Figure 10: ***Field visualization.*** *This set of figures compares visualization of a field on the boundary of a solid using dense meshes and the B-rep SE. (a) Shows a solid approximated by a dense mesh containing more than 98K triangles. Without* a priori *knowledge of the field, a dense mesh is required to ensure sampling at the mesh vertices accurately captures the spatial frequencies inherent in the field. (b) Illustrates the resulting field visualization. Comparison of (a) and (b) reveals that many triangles are used in regions where the field is largely uniform. (c) Shows the same solid approximated by a mesh containing 6K triangles, refined adaptively using a sample spacing more than ten times finer than the spacing available with the fine mesh in (a). (d) Shows the resulting field visualization which is indistinguishable from (b).*

ure 11 shows, the geometry can possess curvature in regions where the field is constant or varying linearly. Likewise, in regions where the field is varying, the geometry may be planar or curved in only one direction. Thus, if we only adapt to the geometry, the spatial variation in the field will not be accurately conveyed. And, if we only adapt to the field, the curvature of the geometry will not be captured.

3.3. Surface Integration

Surface integral computation arises frequently in engineering in the solution of analyses requiring satisfaction of boundary conditions on a solid's surfaces and in the calculation of such geometric properties as volume and surface area[LR82]. These integrals all take on the following form:

$$I = \int_{\Omega} f d\Omega, \tag{1}$$

where Ω is the domain of integration and f is a scalar function of spatial variables whose integral we are interested in computing. For surface integration, Ω is a solid boundary, and f may be pressure, or energy flux. For volume integration, the problem can often be reduced to boundary integration using Stokes theorem [LR82]. Polynomial functions can be integrated exactly over polyhedral geometry [CP90] or over domains bounded by polynomial surfaces [GOMP98]. However, due to high cost, the general curved domains encountered in engineering, and the fact the integrands are frequently not known *a priori*, computation of (1) must be performed numerically.

Numerical solution of (1) requires two deceptively simple steps: one, generate sample points x_i on Ω; two, assign weights W_i for each $f(x_i)$ and sum. The schemes by which points and weights are allocated are known as *quadrature rules*. Such rules exist for standardized planar regions with weights assigned to guarantee exact integration of polynomials up to the

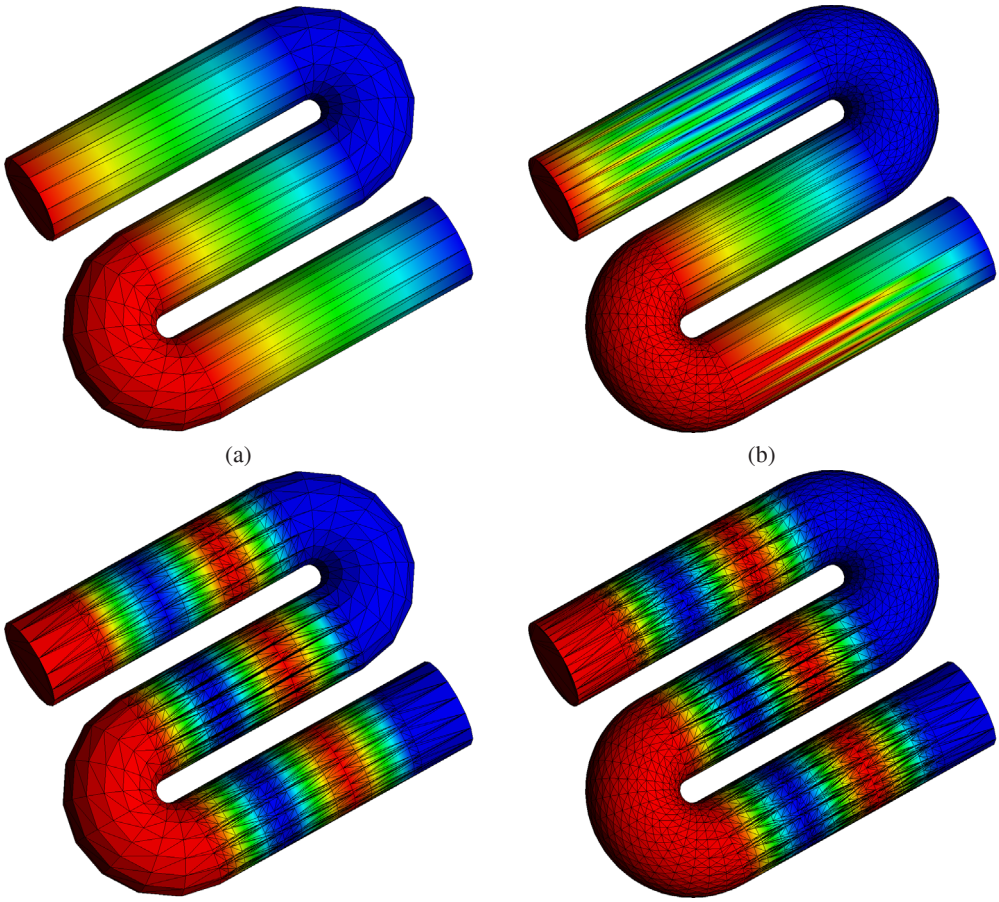

Figure 11: ***Adaptation to both fields and geometry.****(a) Shows a coarse, flat-shaded, mesh approximation of an S-shaped pipe with a spatially varying field with sinusoidal variation in the central, straight portions and constant value in the end regions. (b) Shows adaptation of the mesh to the* exact geometry only. *Notice that the mesh density is greatest in the regions where the curvature of the geometry is greatest; however, the spatial variation of the field is not accurately captured by the long triangles in the central portion. On the other hand, (c) shows adaptation of the mesh to the incident* field only. *There is a concentration of triangles in the central portion that provides an accurate rendition of the field; however, the accuracy of the mesh in the bends is unchanged from the original mesh in (a). (d) Shows the results of refinement that accounts for both geometric error and error in the field interpolation. Notice that compared to (c), the bends in the pipe are approximated more closely with smaller triangles, while the field interpolation in the central regions is unchanged.*

degree of the rule. We can use various representations for Ω, each with tradeoffs.

The customary approach to the numerical solution of (1) is to represent Ω by a triangular mesh and use standard triangle quadrature rules to compute the integral. With this technique, the accuracy of the mesh approximation limits the accuracy with which the integral can be computed. The only quadrature rule that uses precisely the vertices of the triangles is only first order accurate. Higher order rules and subdivision of the mesh introduce sampling error where the exact geometry is non-planar. The only way to decrease the integration error with a mesh is to generate many small triangles at the outset, gaining accuracy at the expense of increased storage and processing time.

We can avoid the inaccuracies inherent in quadrature over meshes by using the exact geometry of the solid's faces in the B-rep. The integration of a function over such parametric surfaces is a well studied problem, taking on the following form:

$$I = \int_{\sigma} f(\Phi(u,v)) \left\| \frac{\partial \Phi}{\partial u} \times \frac{\partial \Phi}{\partial v} \right\| du dv \qquad (2)$$

The parametric surface equation is Φ and $\left\| \frac{\partial \Phi}{\partial u} \times \frac{\partial \Phi}{\partial v} \right\|$ is the Jacobian of the parameterization. When computing (2) numerically, we apply quadrature rules in parametric space, sam-

pling the integrand f at points on the solid boundary evaluated through Φ. Multiplication by the Jacobian accounts for the distortion that occurs when mapping from parametric space to $\mathbb{E}^3$. This is especially effective when Ω is the union of untrimmed parametric surface patches [GOMP98]. However, since the faces of the solid are represented by *trimmed* surface patches with arbitrary topology and geometry, we must decompose the parametric domain into primitive regions. Moreover, such decompositions can be subdivided to decrease the sample spacing in $\mathbb{E}^3$, thus increasing the accuracy of the integral. By generating points through the surface equation, we circumvent the problem of inaccurate sampling so the use of high order rules is possible and the integrand is always evaluated on the exact geometry.

Two common choices for primitive regions are rectangles and triangles. Quadrature with rectangles relies on quadtree decomposition of the parametric domain, which is effective in most circumstances [TS02]. When use of quadtrees is not acceptable (due to speed, accuracy, or representational constraints), quadrature with the B-rep SE combines the simplicity of mesh-based integration with the accuracy of the parametric surface approach. With the B-rep SE the simplicial structure is used to address the cells of the boundary as simply as with a mesh. Quadrature rules are then applied through a parameterization of the simplexes' exact embedding functions. The use of the embedding functions generates points on the exact boundary where f is evaluated, weighted, and summed. The weight for each point is the product of the quadrature weight and a *weight modifier* that is the Jacobian of the parameterized embedding function. When the embedding function is Φ, the integral is precisely (2). However, unlike parametric surface integration, with B-rep SE specific knowledge of the solid data structure is not assumed, and special processing for arbitrarily shaped faces is not required. Finally, in contrast with meshes, integral accuracy can be adaptively increased based on properties of the geometry, the integrand, or both.

4. Conclusions

In this paper we have proposed the B-rep SE, a hybrid data structure that combines the attractive properties of both triangular meshes and exact B-reps; sacrificing neither the speed of meshes nor the accuracy of the exact B-rep. The B-rep SE can be viewed as a traditional triangular mesh extended with arbitrary resolution, or as a B-rep enhanced with simplicial subdivision capabilities. Currently implemented as an API, it conveniently hides the complexity of the conventional boundary representation by allowing access to the solid boundary in a mesh-like manner. Other meshing and visualization APIs implement partial or limited functionality of the B-rep SE. For example, CAPRI[ADH99, HF98] provides a restricted interface to boundary representations that requires a valid mesh at all times and relies on heuristics for correspondence. The validity conditions on the B-rep SE (Def. 1) are relatively mild, but assume the ability to overcome the usual difficulties with seams and degeneracies in boundary representations[dCS96].

There is a wealth of unexplored applications for the B-rep SE. In industries that rely heavily on solid modeling, mesh approximations of parts at multiple resolutions are routinely being generated, stored, and transmitted for enterprise-wide visualization. With the B-rep SE, it should be possible to make the storage and transmission tasks superfluous through online generation of meshes at the point of use. The computational overhead of maintaining the simplicial structure of the B-rep SE is no more severe than the overhead of generating the meshes used for rendering during interactive modeling sessions. The simplicial enhancement only requires the retention of the parametric triangulations that form the pre-image of these rendering meshes. Further, the memory overhead for storing the simplicial structure can be minimized by application of coarsening steps.

The structure, as presented, relies on parametric surface definitions, but it should be possible to extend it to cover other surface descriptions such as subdivision and implicit surfaces as well. In the case of subdivision surfaces, the minimal simplicial enhancement could be taken from the coarsest control mesh and techniques such as described in [Sta98] might allow computation of the exact embedding without explicit subdivision according to the surface's subdivision rule. It may be possible to provide simplicial enhancement of implicit surfaces starting from a mesh approximation and using correspondences defined using such geometric measures as nearest-point or line-surface intersection. Of course introduction of such correspondences raises concerns about bijectivity of the correspondence mappings. Alternatively, we might specify that the implicit surfaces be *normalform functions* so that points on an approximation of the embedding have *foot points* on the surface[Har00]. In such formulations, evaluation of the implicit equation yields a signed distance to the zero set of the function while the gradient provides the direction.

As suggested in Figure 6, the B-rep SE can be used with other constructions for approximating embeddings. For example, instead of using a single planar triangle to approximate the embedding of a 2-simplex from A, a hierarchy of meshes could be constructed with each level more closely approximating the exact surface. Another obvious extension is to use higher-order polynomials to approximate the embedding of simplexes from A. This would provide better control of the error between the embedding $g^*(A)$ and it's approximations.

We chose the simplicial structure to consist of a complex of triangular simplexes because visualization requires coherency of geometry across edges, and triangles are easily manipulated to maintain this coherency. Tasks such as surface integration for which coherency may not be an issue, might make use of other types of cellular enhancements. One can envision *quadtree* (B-rep QE) or *extended-quadtree*[ABJN85] (B-rep EQE) enhanced B-reps that decompose S into nominally rectangular regions.

We have focused on point membership and generation tasks, but most geometric computations (set membership classification in particular) reduce to a finite number of such point tasks[Sha02]. Hence, simplicial enhancement of B-reps is generally useful and it may be worthwhile to study other algorithms in detail.

Acknowledgments

This work was supported in part by the National Science Foundation grants DMI-9900171, DMI-0115133, DMI-0323514, and CCR-0112758; General Motors Corporation; EDS PLM Solutions; and NIST Grant 60NANB2D0126.

References

[ABJN85] AYALA D., BRUNET P., JUAN R., NAVAZO I.: Object representation by means of nonminimal division quadtrees and octrees. *ACM Transactions on Graphics 4*, 1 (1985), 41–59. 10

[ADH99] AFTOSMIS M. J., DELANAYE M., HAIMES R.: Automatic generation of cfd-ready surface triangulations from cad geometry. *AIAA Paper 99-0776* (January 1999). 10

[BST03] BISWAS A., SHAPIRO V., TSUKANOV I.: Heterogeneous material modeling with distance fields. *Computer-Aided Geometric Design 21*, 3 (2003), 215–242. 7

[Cai68] CAIRNS S. S.: *Introductory Topology*. Ronald Press, New York, 1968. 3

[CB97] CHEN H., BISHOP J.: Delaunay triangulations for curved surfaces. In *Proceedings of the 6th International Meshing Roundtable, Sandia National Laboratories* (October 1997), pp. 115–127. 1

[CLR90] CORMEN T. H., LEISERSON C. E., RIVEST R. L.: *Introduction to Algorithms*. MIT Press, Cambridge, MA, 1990. 2

[CP90] CATTANI C., PAOLUZZI A.: Boundary integration over linear polyhedra. *Computer-Aided Design 22*, 2 (March 1990), 130–135. 8

[dCS96] DE COUGNY H. L., SHEPARD M. S.: *Surface Meshing Using Vertex Insertion*. Technical report, RPI, 1996. 10

[FK90] FORSEY D. R., KLASSEN V.: An adaptive subdivision algorithm for crack prevention in the display of parametric surfaces. In *Proceedings of Graphics Interface* (1990), pp. 1–8. 1

[FP95] FLORIANI L. D., PUPPO E.: Hierarchical triangulation for multiresolution surface description. *ACM Transactions on Graphics 14*, 4 (October 1995), 363–411. 2

[FTU95] FEITO F., TORRES, URENA: Orientation, simplicity and inclusion test for planar polygons. *Computers and Graphics 19* (1995), 595–600. 2

[GH97] GARLAND M., HECKBERT P.: Surface simplification using quadric error metrics. In *Proceedings of the 24th Annual Conference on Computer Graphics* (1997), pp. 202–216. 6

[GH98a] GARLAND M., HECKBERT P.: Multiresolution modeling: Survey and future opportunities. In *Eurographics '99, State of the Art Report* (September 1998). 2

[GH98b] GARLAND M., HECKBERT P.: Simplifying surfaces with color and texture using quadric error metrics. In *Proceedings of IEEE Visualization '98* (1998), pp. 263–269. 7

[GOMP98] GONZALEZ-OCHOA C., MCCAMMON S., PETERS J.: Computing moments of objects enclosed by piecewise polynomial surfaces. *ACM Transactions on Graphics 17*, 3 (1998), 143–157. 8, 10

[Har00] HARTMANN E.: Numerical parameterization of curves and surfaces. *Computer Aided Geometric Design* (2000), 251–266. 10

[HF98] HAIMES R., FOLLEN G. J.: Computational Analysis PRogramming Interface. In *Proceedings of the 6th International Conference on Numerical Grid Generation in Computational Fluid Simulations, University of Greenwich, United Kingdom* (July 1998). 10

[Hop96] HOPPE H.: Progressive meshes. In *SIGGRAPH '96 Proc.* (August 1996), pp. 99–108. 2

[Hop99] HOPPE H.: New quadric metric for simplifying meshes with appearance attributes. *IEEE Visualization* (October 1999), 59–66. 7

[HY88] HOCKING J. G., YOUNG G. S.: *Topology*. Dover Publications, New York, 1988. 3

[KS95] KLEIN R., STRASSER W.: Large mesh generation from boundary models with parametric face representation. In *Proceedings of the Third Symposium on Solid Modeling and Applications* (1995), pp. 431–440. 1

[KSSP01] KUMAR G. V. V. R., SRINIVASAN P., SHASTRY K. G., PRAKASH B. B.: Geometry based triangulation of multiple trimmed nurbs surfaces. *Computer Aided Design* (2001), 439–454. 1

[Lee00] LEE J. M.: *Introduction to Topological Manifolds*. Springer-Verlag, New York, 2000. 3

[LR82] LEE Y. T., REQUICHA A. A.: Algorithms for computing the volume and other integral properties of solids. i. known methods and open issues. *Communications of the ACM 25*, 9 (September 1982), 635–641. 8

[Mau80] MAUNDER C. R. F.: *Algebraic Topology*. Dover Publications, Inc., Mineola, New York, 1980. 3

[MM97] MUKHERJEE Y. X., MUKHERJEE S.: The boundary node method for potential problems. *International Journal for Numerical Methods in Engineering 40* (1997), 797–815. 1

[Mor97] MORTENSON M. E.: *Geometric Modeling*. John Wiley and Sons, Inc., New York, 1997. 1

[O'R98] O'ROURKE J.: *Computational Geometry in C*. Cambridge University Press, Cambridge, United Kingdom, 1998. 2

[Pet94] PETERSON J. W.: *Graphics Gems IV*. Academic Press, Inc., 1994, ch. Tessellation of NURB Surfaces, pp. 286–320. 1

[Req77] REQUICHA A.: *Mathematical Models of Rigid Solid Objects*. Technical Memo 28, Production Automation Project, University of Rochester, Rochester, NY, November 1977. 3

[RHD89] ROCKWOOD A., HEATON K., DAVIS T.: Real-time rendering of trimmed surfaces. *Computer Graphics 23*, 3 (1989), 107–116. 1

[Sab01] SABIN M.: Subdivision: Tutorial notes. Course notes for SMI2001, Genoa., May 2001. 2

[Sab02] SABIN M.: Subdivision surfaces. In *Handbook of Computer Aided Geometric Design*, Farin G., Hoschek J.,, eds. M.-S. K., (Eds.). Elsevier Science Publishers, 2002. 2, 3

[Sam84] SAMET H.: The quadtree and related hierarchical data structures. *ACM Computing Surveys 16*, 2 (1984), 187–260. 1

[SH93] SHENG X., HIRSCH B.: Triangulation of trimmed surfaces in parametric space. *Computer-Aided Design 24*, 8 (August 1993), 437–444. 1

[Sha02] SHAPIRO V.: Solid modeling. In *Handbook of Computer Aided Geometric Design*, Farin G., Hoschek J.,, eds. M.-S. K., (Eds.). Elsevier Science Publishers, 2002. 10

[Sta98] STAM J.: Exact evaluation of catmull-clark subdivision surfaces at arbitrary parameter values. In *Computer Graphics Proceedings, Annual Conference Series* (July 1998), pp. 395–404. 10

[SYI97] SHIMADA K., YAMADA A., ITOH T.: Anisotropic triangular meshing of parametric surfaces via close packing of ellipsoidal bubbles. In *Proceedings of the 6th International Meshing Roundtable, Sandia National Laboratories* (October 1997), pp. 375–390. 1

[SZD*98] SCHRÖDER P., ZORIN D., DEROSE T., FORSEY D. R., KOBBELT L., LOUNSBERY M., PETERS J.: Subdivision for modeling and animation. Course notes for SIGGRAPH 98, July 1998. 2

[TS02] TSUKANOV I., SHAPIRO V.: The architecture of SAGE - A meshfree system based on RFM. *Engineering with Computers 18*, 4 (2002), 295–311. 7, 10

[UGS] UGS PLM SOLUTIONS: Parasolid. Software. 3

[VB93] VIGO M., BRUNET P.: Piecewise linear approximation of trimmed surfaces. In *Geometric Modeling*, Farin G., Hagen H.,, Noltemeier H., (Eds.). Springer-Verlag, 1993. 1

[VdFG99] VELHO L., DE FIGUEIREDO L. H., GOMES J.: A unified approach for hierarchical adaptive tessellation of surfaces. *ACM Transactions on Graphics 18*, 4 (October 1999), 329–360. 6